Structure factors and quantum geometry in multiband BCS superconductors

M. Iskin
Department of Physics, Koç University, Rumelifeneri Yolu, 34450 Sarıyer, Istanbul, Türkiye
(Dated: July 14, 2025)

We consider multiband BCS superconductors that exhibit time-reversal symmetry and uniform pairing, and analyze their dynamic density and spin structure factors using linear-response theory within the mean-field BCS-BEC crossover framework at zero temperature. Our results for the multi-orbital Hubbard model satisfy the associated f-sum rules in several limits. In particular, in the strong-coupling limit, they coincide with those of a weakly-interacting Bose gas of Cooper pairs, where the low-energy collective Goldstone modes serve as Bogoliubov phonons. We further reveal that the quantum-geometric origin of the low-energy structure factors, along with related observables such as the superfluid-weight tensor and the effective-mass tensor of Cooper pairs, can be traced all the way back to the effective-mass theorem for Bloch bands in this limit. As an illustration, we investigate the pyrochlore-Hubbard model numerically and demonstrate that the Goldstone modes are the only relevant collective degrees of freedom in the flat-band regime.

I. INTRODUCTION

Advances in solid-state and condensed-matter physics have increasingly demonstrated the importance of quantum geometry in understanding and controlling the behavior of multiband systems [1–10]. Central to this perspective is the complex quantum-geometric tensor [11–13], whose imaginary part, i.e., the Berry-curvature tensor, has long been recognized for its role in defining topological invariants such as the Chern number. This invariant not only classifies topological phases of matter but also governs transport phenomena in materials ranging from topological insulators to unconventional superconductors. Equally compelling is the real part of the quantum-geometric tensor, i.e., the quantum-metric tensor, which quantifies the quantum distance between nearby Bloch states. While historically less explored than its Berry-curvature counterpart, the quantum metric has emerged as a crucial factor in a variety of physical contexts [14–17]. In multiband superconductors, for example, it mediates virtual interband processes that endow Cooper pairs with a finite effective mass even in systems where an isolated flat band would otherwise preclude superconductivity due to an infinite band mass. This geometric mechanism thus provides a natural explanation for the emergence of superconductivity in flat-band systems, linking key observables such as the superfluid weight, critical temperature, coherence length, pair size and low-energy collective modes. For an extended bibliography on this topic, see the recent reviews [14–17].

The interplay between conventional band-dispersion effects and these geometric contributions becomes particularly pronounced in nearly flat bands, where the former terms are suppressed. Recent theoretical work, spanning from one-dimensional to three-dimensional tight-binding toy models has solidified the notion that nontrivial band geometry is indispensable for realizing superconductivity in flat-band materials [14–17]. By integrating both topological and geometric insights, this emerging framework challenges conventional BCS paradigms and opens new avenues for designing high-critical-temperature superconductors. Ultimately, the synthesis of quantum-geometric concepts with traditional band theory offers a unified perspective on superconducting pairing, illuminating the subtle yet profound influence of band geometry on the macroscopic properties of quantum materials. Thus, motivated by recent studies on the static structure factor of band insulators [18, 19], here we utilize linear-response theory within the mean-field BCS-BEC crossover framework at zero temperature, and examine the dynamic density structure factor (DSF) and dynamic spin structure factor (SSF) of multiband BCS superconductors that exhibit time-reversal symmetry and uniform pairing. Our analysis of the multi-orbital Hubbard model reveals that the collective-mode contribution to the spectral function of the density response is directly related to the superfluid-weight tensor. In the strong-coupling limit, they align with those of a weakly interacting Bose gas of Cooper pairs, where the low-energy collective Goldstone modes serve as Bogoliubov phonons. Furthermore, we show that the quantum-geometric origins of the low-energy structure factors, superfluid-weight tensor and the effective-mass tensor of Cooper pairs can all be traced back to the effective-mass theorem for Bloch bands in this limit.

The remainder of the paper is organized as follows. In Sec. II, we introduce the density and spin response functions, along with their associated structure factors and f-sum rules, for a generic multi-orbital Hubbard model. In Sec. III, we discuss the zero-temperature linear-response theory for multiband BCS superconductors and analyze the structure factors within the mean-field BCS-BEC crossover framework. In Sec. IV, we present numerical calculations for the pyrochlore-Hubbard model. In Sec. V, we comment on the role of Coulomb interactions on the low-lying collective excitations. The paper concludes with a summary in Sec. VI, while a brief discussions of the effective Gaussian action, the Ward identities, and the effective-mass tensors are provided in the Appendix.

II. CORRELATION FUNCTIONS

The linear density-response function $\mathcal{X}(\mathbf{r},t) = -i\theta(t)\langle[\rho(\mathbf{r},t),\rho(\mathbf{0},0)]\rangle$ measures the correlation between the density of particles at two different points, where $\theta(t)$ is the Heaviside step function, $\langle\cdots\rangle$ represents the thermal statistical average, and $\rho(\mathbf{r},t) = \rho_\uparrow(\mathbf{r},t) + \rho_\downarrow(\mathbf{r},t)$ is the total density operator in the Heisenberg picture [20]. Its spatial Fourier transform is given by $\mathcal{X}(\mathbf{q},t) = \frac{1}{\sqrt{V}}\int d^3\mathbf{r}e^{-i\mathbf{q}\cdot\mathbf{r}}\mathcal{X}(\mathbf{r},t)$, which can be obtained using $\rho(\mathbf{r},t) = \frac{1}{\sqrt{V}}\sum_{\mathbf{q}} e^{i\mathbf{q}\cdot\mathbf{r}}\rho(\mathbf{q},t)$ along with $\int d^3\mathbf{r}e^{i(\mathbf{q}-\mathbf{q}')\cdot\mathbf{r}} = V\delta_{\mathbf{q}\mathbf{q}'}$. Here, V is the volume of the system and δ_{ij} is a Kronecker delta. The spectral function of its spatio-temporal Fourier transform,

$$\mathcal{X}(\mathbf{q},\omega) = -i\int_0^\infty dt e^{i\omega t}\langle[\rho(\mathbf{q},t),\rho(-\mathbf{q},0)]\rangle, \quad (1)$$

determines the dynamic and static DSFs as follows.

A. Density structure factor (DSF)

The imaginary part of the density response function is related to the dynamic DSF $S(\mathbf{q},\omega)$ through $\mathrm{Im}\mathcal{X}(\mathbf{q},\omega+i0^+) = -\pi[S(\mathbf{q},\omega) - S(-\mathbf{q},-\omega)]$, where $S(\mathbf{q},-\omega) = e^{-\beta\omega}S(\mathbf{q},\omega)$ is the so-called detailed balance [20]. Throughout this paper, we assume inversion symmetry and set $S(-\mathbf{q},\omega) = S(\mathbf{q},\omega)$, which leads to $S(\mathbf{q},\omega) = -\frac{1}{\pi}\frac{\mathrm{Im}\mathcal{X}(\mathbf{q},\omega+i0^+)}{1-e^{-\beta\omega}}$, where $\beta = 1/T$ is the inverse temperature in units of $\hbar = k_B = 1$ the Planck and Boltzmann constants. Furthermore, at zero temperature (of interest in this paper), one finds [20]

$$S(\mathbf{q},\omega) = -\frac{1}{\pi}\mathrm{Im}\mathcal{X}(\mathbf{q},\omega+i0^+) \quad (2)$$

for $\omega > 0$, and $S(\mathbf{q},\omega) = 0$ for $\omega < 0$. By plugging $\rho(\mathbf{q},t) = e^{i\mathcal{H}t}\rho_{\mathbf{q}}e^{-i\mathcal{H}t}$ into Eq. (1), where $\rho_{\mathbf{q}} = \rho_{\uparrow\mathbf{q}} + \rho_{\downarrow\mathbf{q}}$ is the Fourier transform of the total density operator at $t = 0$, and $\mathcal{H}$ is the Hamiltonian that governs the system, and using the Schrödinger equation $\mathcal{H}|\phi_\mathcal{N}\rangle = \mathcal{E}_\mathcal{N}|\phi_\mathcal{N}\rangle$ for the stationary states along with the completeness relation $\sum_\mathcal{N}|\phi_\mathcal{N}\rangle\langle\phi_\mathcal{N}| = 1$, we find $\mathrm{Im}\mathcal{X}(\mathbf{q},\omega+i0^+) = -\pi\sum_\mathcal{N}[|\langle\phi_0|\rho_{\mathbf{q}}|\phi_\mathcal{N}\rangle|^2\delta(\omega-\mathcal{E}_\mathcal{N}+\mathcal{E}_0) - |\langle\phi_0|\rho^\dagger_{\mathbf{q}}|\phi_\mathcal{N}\rangle|^2\delta(\omega+\mathcal{E}_\mathcal{N}-\mathcal{E}_0)]$ at $T = 0$. Here, $|\phi_0\rangle$ represents the ground state and we make use of the identity $1/(x+i0^+) = \mathcal{P}(\frac{1}{x}) - i\pi\delta(x)$, with $\mathcal{P}$ denoting the Cauchy principal value and $\delta(x)$ the Dirac delta function. Thus, the dynamic DSF is simply given by $S(\mathbf{q},\omega) = \sum_\mathcal{N}|\langle\phi_0|\rho_{\mathbf{q}}|\phi_\mathcal{N}\rangle|^2\delta(\omega-\mathcal{E}_\mathcal{N}+\mathcal{E}_0)$, leading to the so-called f-sum rule $\int_0^\infty d\omega\omega S(\mathbf{q},\omega) = \sum_\mathcal{N}(\mathcal{E}_\mathcal{N}-\mathcal{E}_0)|\langle\phi_0|\rho_{\mathbf{q}}|\phi_\mathcal{N}\rangle|^2$. It is easy to show that $\langle\phi_0|[\rho^\dagger_{\mathbf{q}},[\rho_{\mathbf{q}},\mathcal{H}]]|\phi_0\rangle = -\sum_\mathcal{N}(\mathcal{E}_\mathcal{N}-\mathcal{E}_0)[|\langle\phi_0|\rho_{\mathbf{q}}|\phi_\mathcal{N}\rangle|^2 + |\langle\phi_0|\rho^\dagger_{\mathbf{q}}|\phi_\mathcal{N}\rangle|^2]$ in general, where $\rho^\dagger_{\mathbf{q}} = \rho_{-\mathbf{q}}$, and this can be expressed as [20]

$$\langle\phi_0|[\rho^\dagger_{\mathbf{q}},[\rho_{\mathbf{q}},\mathcal{H}]]|\phi_0\rangle = -2\int_0^\infty d\omega\omega S(\mathbf{q},\omega) \quad (3)$$

in the presence of inversion symmetry. Furthermore, the static DSF $S(\mathbf{q})$ is defined by $\int_0^\infty S(\mathbf{q},\omega)d\omega = \langle\phi_0|\rho_{\mathbf{q}}\rho^\dagger_{\mathbf{q}}|\phi_0\rangle = \frac{n_0}{2}S(\mathbf{q})$, where n_0 is the total density of particles [21, 22].

B. Spin structure factor (SSF)

Similar to Eq. (1), we define the linear spin-response function for the spin-density operator $\rho_s(\mathbf{r},t) = \rho_\uparrow(\mathbf{r},t) - \rho_\downarrow(\mathbf{r},t)$ as $\mathcal{X}_s(\mathbf{q},\omega) = -i\int_0^\infty dt e^{i\omega t}\langle[\rho_s(\mathbf{q},t),\rho_s(-\mathbf{q},0)]\rangle$, which leads to $S_s(\mathbf{q},\omega) = -\frac{1}{\pi}\mathrm{Im}\mathcal{X}_s(\mathbf{q},\omega+i0^+)$ for $\omega > 0$, and $S_s(\mathbf{q},\omega) = 0$ for $\omega < 0$ at $T = 0$. It is easy to show that $[\rho^\dagger_{s\mathbf{q}},[\rho_{s\mathbf{q}},\mathcal{H}]] = [\rho^\dagger_{\mathbf{q}},[\rho_{\mathbf{q}},\mathcal{H}]]$ for the operator $\rho_{s\mathbf{q}} = \rho_{\uparrow\mathbf{q}} - \rho_{\downarrow\mathbf{q}}$, leading to the spin f-sum rule [22, 23]

$$\int_0^\infty d\omega\omega S_s(\mathbf{q},\omega) = \int_0^\infty d\omega\omega S(\mathbf{q},\omega). \quad (4)$$

Alternatively, one can define the spin-resolved dynamic structure factors [21, 24] $S_{\sigma\sigma'}(\mathbf{q},\omega) = \sum_\mathcal{N}\langle\phi_0|\rho_{\sigma\mathbf{q}}|\phi_\mathcal{N}\rangle\langle\phi_\mathcal{N}|\rho^\dagger_{\sigma'\mathbf{q}}|\phi_0\rangle\delta(\omega - \mathcal{E}_\mathcal{N} + \mathcal{E}_0)$, and identify $S(\mathbf{q},\omega) = \sum_{\sigma\sigma'}S_{\sigma\sigma'}(\mathbf{q},\omega)$ as the dynamic DSF and $S_s(\mathbf{q},\omega) = \sum_{\sigma\sigma'}(-1)^{1+\delta_{\sigma\sigma'}}S_{\sigma\sigma'}(\mathbf{q},\omega)$ as the dynamic SSF. It is expected that $S_{\uparrow\uparrow}(\mathbf{q},\omega) = S_{\downarrow\downarrow}(\mathbf{q},\omega)$ and $S_{\uparrow\downarrow}(\mathbf{q},\omega) = S_{\downarrow\uparrow}(\mathbf{q},\omega)$ in the presence of time-reversal and inversion symmetries, which are assumed to be the case in this paper. This suggests that $\int_0^\infty d\omega\omega S_{\uparrow\downarrow}(\mathbf{q},\omega) = 0$ [22]. Furthermore, $\langle\phi_0|[\rho^\dagger_{\sigma\mathbf{q}},[\rho_{\sigma'\mathbf{q}},\mathcal{H}]]|\phi_0\rangle = -\int_0^\infty d\omega\omega[S_{\sigma\sigma'}(-\mathbf{q},\omega) + S_{\sigma'\sigma}(\mathbf{q},\omega)]$ in general, and the static SSF $S_s(\mathbf{q})$ is defined by $\int_0^\infty S_s(\mathbf{q},\omega)d\omega = \langle\phi_0|\rho_{s\mathbf{q}}\rho^\dagger_{s\mathbf{q}}|\phi_0\rangle = \frac{n_0}{2}S_s(\mathbf{q})$ [21, 22].

C. F-sum rule in a multi-orbital Hubbard model

Next, we consider a multiband tight-binding lattice that is described by the Bloch Hamiltonian matrix $\mathbf{h}_{\mathbf{k}\sigma}$, which satisfies the Schrödinger equation $\mathbf{h}_{\mathbf{k}\sigma}|n_{\mathbf{k}\sigma}\rangle = \varepsilon_{n\mathbf{k}\sigma}|n_{\mathbf{k}\sigma}\rangle$ for the periodic part $|n_{\mathbf{k}\sigma}\rangle$ of the Bloch states. Here, the dispersion relation $\varepsilon_{n\mathbf{k}\sigma}$ for the nth Bloch band is determined by the eigenvalue relation

$$\sum_{S'} h^{SS'}_{\mathbf{k}\sigma}n_{S'\mathbf{k}\sigma} = \varepsilon_{n\mathbf{k}\sigma}n_{S\mathbf{k}\sigma}, \quad (5)$$

where $n_{S\mathbf{k}\sigma} = \langle S|n_{\mathbf{k}\sigma}\rangle$ is the projection to the Sth sublattice in a unit cell. The precise form of the matrix elements $h^{SS'}_{\mathbf{k}\sigma}$ depends on the lattice geometry and hopping parameters. Suppose the operator $c^\dagger_{Si\sigma}$ creates a spin-σ fermion in the ith unit cell on sublattice $S \in \{A,B,C,\cdots\}$. Then, the corresponding site operator for the number of spin-σ fermions is given by $\rho_{Si\sigma} = c^\dagger_{Si\sigma}c_{Si\sigma}$. Using the discrete Fourier transforms $c_{Si\sigma} = \frac{1}{\sqrt{N_c}}\sum_{\mathbf{k}} e^{i\mathbf{k}\cdot\mathbf{r}_{Si}}c_{S\mathbf{k}\sigma}$ and $\rho_{S\mathbf{q}\sigma} = \frac{1}{\sqrt{N_c}}\sum_{\mathrm{i}} e^{-i\mathbf{q}\cdot\mathbf{r}_{Si}}\rho_{Si\sigma}$, where N_c is the number of unit cells in the system and $\mathbf{r}_{Si}$ is the position of the lattice site $S \in \mathrm{i}$, and performing

a basis transformation from the sublattice to the band basis through $c^\dagger_{S\mathbf{k}\sigma} = \sum_n n^*_{S\mathbf{k}\sigma} c^\dagger_{n\mathbf{k}\sigma}$, we obtain

$$\rho_{S\mathbf{q}\sigma} = \frac{1}{\sqrt{N_c}} \sum_{nm\mathbf{k}} n^*_{S,\mathbf{k}-\mathbf{q},\sigma} m_{S\mathbf{k}\sigma} c^\dagger_{n,\mathbf{k}-\mathbf{q},\sigma} c_{m\mathbf{k}\sigma}. \tag{6}$$

Here, we also used $\sum_{\mathrm{i}} e^{i(\mathbf{q}-\mathbf{q}')\cdot\mathbf{r}_{S\mathrm{i}}} = N_c \delta_{\mathbf{q}\mathbf{q}'}$. Note that $\rho^\dagger_{S\mathbf{q}\sigma} = \rho_{S,-\mathbf{q},\sigma}$, and $\rho_{\mathbf{q}} = \sum_{S\sigma} \rho_{S\mathbf{q}\sigma}$ for the density operator and $\rho_{s\mathbf{q}} = \sum_S (\rho_{S\mathbf{q}\uparrow} - \rho_{S\mathbf{q}\downarrow})$ for the spin-density operator. As a result, the multi-orbital Hubbard model $\mathcal{H} = \mathcal{H}_0 + \mathcal{H}_I$ with onsite attractive interactions $U \geq 0$, i.e., $\mathcal{H}_0 = -\sum_{S\mathrm{i};S'\mathrm{i}';\sigma} t^\sigma_{S\mathrm{i};S'\mathrm{i}'} c^\dagger_{S\mathrm{i}\sigma} c_{S'\mathrm{i}'\sigma}$ and $\mathcal{H}_I = -U \sum_{S\mathrm{i}} \rho_{S\mathrm{i}\uparrow}\rho_{S\mathrm{i}\downarrow}$, can be equivalently written as

$$\mathcal{H}_0 = \sum_{SS'\mathbf{k}\sigma} c^\dagger_{S\mathbf{k}\sigma} (h^{SS'}_{\mathbf{k}\sigma} - \mu\delta_{SS'}) c_{S'\mathbf{k}\sigma}, \tag{7}$$

$$\mathcal{H}_I = -U \sum_{S\mathbf{q}} \rho_{S\mathbf{q}\uparrow}\rho_{S,-\mathbf{q},\downarrow}, \tag{8}$$

in momentum space. Here, the hopping parameters $t^\sigma_{S\mathrm{i};S'\mathrm{i}'}$ describe tunneling of a spin-σ particle from the sublattice site $S' \in \mathrm{i}'$ to the sublattice site $S \in \mathrm{i}$, $h^{SS'}_{\mathbf{k}\sigma} = -\frac{1}{N_c}\sum_{\mathrm{i}\mathrm{i}'} t^\sigma_{S\mathrm{i};S'\mathrm{i}'} e^{\mathrm{i}\mathbf{k}\cdot\mathbf{r}_{S\mathrm{i};S'\mathrm{i}'}}$ with $\mathbf{r}_{S\mathrm{i};S'\mathrm{i}'} = \mathbf{r}_{S'\mathrm{i}'} - \mathbf{r}_{S\mathrm{i}}$ denoting the relative position, and μ is the chemical potential.

In order to make analytical progress with the f-sum rule, we first note that $[\rho_{S\mathbf{q}\sigma}, \rho_{S'\mathbf{q}'\sigma'}] = 0$ leading to $[\rho_{S\mathbf{q}\sigma}, \mathcal{H}_I] = 0$. Then, after some simple algebra [25], we find

$$[\rho^\dagger_{\mathbf{q}}, [\rho_{\mathbf{q}}, \mathcal{H}]] = \frac{1}{N_c} \sum_{nml\mathbf{k}\sigma} (\varepsilon_{m\mathbf{k}\sigma} - \varepsilon_{n,\mathbf{k}-\mathbf{q},\sigma}) \langle n_{\mathbf{k}-\mathbf{q},\sigma}|m_{\mathbf{k}\sigma}\rangle \times \left(\langle l_{\mathbf{k}\sigma}|n_{\mathbf{k}-\mathbf{q},\sigma}\rangle c^\dagger_{l\mathbf{k}\sigma} c_{m\mathbf{k}\sigma} - \langle m_{\mathbf{k}\sigma}|l_{\mathbf{k}-\mathbf{q},\sigma}\rangle c^\dagger_{n,\mathbf{k}-\mathbf{q},\sigma} c_{l,\mathbf{k}-\mathbf{q},\sigma}\right), \tag{9}$$

where $\langle n_{\mathbf{k}\sigma}|m_{\mathbf{k}'\sigma}\rangle = \sum_S n^*_{S\mathbf{k}\sigma} m_{S\mathbf{k}'\sigma}$ and $\langle n_{\mathbf{k}\sigma}|m_{\mathbf{k}\sigma}\rangle = \delta_{nm}$. If only intraband averages are nonzero with respect to the ground state, i.e., $\langle c^\dagger_{n\mathbf{k}\sigma} c_{m\mathbf{k}\sigma}\rangle = \langle c^\dagger_{n\mathbf{k}\sigma} c_{n\mathbf{k}\sigma}\rangle \delta_{nm}$, then we find

$$\langle [\rho^\dagger_{\mathbf{q}}, [\rho_{\mathbf{q}}, \mathcal{H}]]\rangle = -\frac{1}{N_c} \sum_{ijn\mathbf{k}\sigma} (M^{-1}_{n\mathbf{k}\sigma})_{ij} q_i q_j \langle c^\dagger_{n\mathbf{k}\sigma} c_{n\mathbf{k}\sigma}\rangle, \tag{10}$$

$$(M^{-1}_{n\mathbf{k}\sigma})_{ij} = \ddot{\varepsilon}^{ij}_{n\mathbf{k}\sigma} - \sum_{m\neq n} (\varepsilon_{n\mathbf{k}\sigma} - \varepsilon_{m\mathbf{k}\sigma}) g^{nm\mathbf{k}\sigma}_{ij}, \tag{11}$$

in the low-$\mathbf{q}$ limit up to second-order in $\mathbf{q}$, where $\ddot{\varepsilon}^{ij}_{n\mathbf{k}\sigma} = \partial^2\varepsilon_{n\mathbf{k}\sigma}/(\partial k_i \partial k_j)$ [26]. Equation (11) is the so-called effective-mass theorem for the nth Bloch band in a multiband setting [27]. The matrix elements $(M^{-1}_{n\mathbf{k}\sigma})_{ij}$ of the inverse effective-mass tensor are given by $\langle n_{\mathbf{k}\sigma}|\ddot{\mathbf{h}}^{ij}_{\mathbf{k}\sigma}|n_{\mathbf{k}\sigma}\rangle$ [16, 28, 29]. Here,

$$g^{nm\mathbf{k}\sigma}_{ij} = 2\mathrm{Re}\left[\langle \dot{n}^i_{\mathbf{k}\sigma}|m_{\mathbf{k}\sigma}\rangle\langle m_{\mathbf{k}\sigma}|\dot{n}^j_{\mathbf{k}\sigma}\rangle\right] \tag{12}$$

is the band-resolved quantum-metric tensor, where Re denotes the real part of the expression and $|\dot{n}^i_{\mathbf{k}\sigma}\rangle = \partial|n_{\mathbf{k}\sigma}\rangle/\partial k_i$. The quantum-metric tensor of the nth Bloch band can be written as $g^{n\mathbf{k}\sigma}_{ij} = \sum_{m\neq n} g^{nm\mathbf{k}\sigma}_{ij}$ [11–13]. In Sec. III D, where we analyze multiband BCS superconductors, we reveal that the quantum-geometric origin of the superfluid-weight tensor, along with related observables such as the effective-mass tensor of Cooper pairs, coherence length and low-energy structure factors, can be traced back to Eq. (11) in the strong-coupling limit.

Whenever a physical quantity is related to the quantum metric, it is important to carefully consider how the metric depends on the positions of the orbitals. In particular, Eq.(11) explicitly reflects this dependence through the term $g^{nm\mathbf{k}\sigma}_{ij}$. Since this equation appears in other physical contexts as well [16, 28, 29], further investigation is required to fully understand the implications of this dependence. That said, in the rest of this paper, we restrict our analysis to models with time-reversal symmetry and uniform pairing. In these cases, the orbital positions are fixed by symmetry at high-symmetry points, simplifying the situation.

III. LINEAR-RESPONSE THEORY FOR MULTIBAND BCS SUPERCONDUCTORS

To make further analytical progress, we consider a generic multi-ortbital Hubbard model that exhibits time-reversal symmetry and uniform BCS pairing across the underlying sublattices within a unit cell. The former condition requires $\mathbf{h}^*_{-\mathbf{k},\downarrow} = \mathbf{h}_{\mathbf{k}\uparrow} = \mathbf{h}_{\mathbf{k}}$, which leads to $n^*_{S,-\mathbf{k},\downarrow} = n_{S\mathbf{k}\uparrow} = n_{S\mathbf{k}}$ and $\varepsilon_{n,-\mathbf{k},\downarrow} = \varepsilon_{n\mathbf{k}\uparrow} = \varepsilon_{n\mathbf{k}}$. Time-reversal symmetry, along with inversion symmetry, guarantees that for every spin-$\downarrow$ electron in the state $(n, -\mathbf{k})$, there exists a corresponding spin-$\uparrow$ electron in the state $(n, \mathbf{k})$. Consequently, the condensation of spin-singlet Cooper pairs with zero center-of-mass momentum forms the ground state, as in the usual BCS theory. Under these assumptions, there is no interband pairing and only intraband averages remain nonzero with respect to the BCS ground state [30, 31]. For instance, $\langle c^\dagger_{n\mathbf{k}\sigma} c_{m\mathbf{k}\sigma}\rangle = v^2_{n\mathbf{k}}\delta_{nm}$, where the coherence factor is given by $v^2_{n\mathbf{k}} = 1/2 - \xi_{n\mathbf{k}}/(2E_{n\mathbf{k}})$, with $\xi_{n\mathbf{k}} = \varepsilon_{n\mathbf{k}} - \mu$ and $E_{n\mathbf{k}} = \sqrt{\xi^2_{n\mathbf{k}} + \Delta^2_0}$ denoting the dispersion of quasiparticles. Here, Δ_0 is the superconducting order parameter for pairing. Thus, by combining Eqs. (3) and (10), we obtain the f-sum rule for the multiband BCS superconductors,

$$2\int_0^\infty d\omega\omega S(\mathbf{q},\omega) = \frac{1}{N_c}\sum_{ijn\mathbf{k}} (M^{-1}_{n\mathbf{k}})_{ij} q_i q_j \left(1 - \frac{\xi_{n\mathbf{k}}}{E_{n\mathbf{k}}}\right), \tag{13}$$

which is valid in the low-$\mathbf{q}$ limit up to second-order in $\mathbf{q}$. Here, the effective-mass tensor of Bloch bands satisfies $\mathbf{M}_{n,-\mathbf{k},\downarrow} = \mathbf{M}_{n\mathbf{k}\uparrow} = \mathbf{M}_{n\mathbf{k}}$. It is pleasing to see that Eq. (13) recovers the well-known textbook result for the continuum model [20–23].

A. BCS-BEC crossover at $T = 0$

Thanks to time-reversal symmetry and the uniform pairing condition, we define the BCS expectation value $\Delta_{S\mathrm{i}} = U\langle c_{S\mathrm{i}\uparrow} c_{S\mathrm{i}\downarrow}\rangle$ as Δ_0 for every sublattice site S within any unit cell i. Then, within the zero-temperature BCS mean-field theory [32], the parameters Δ_0 and μ are determined by the self-consistent solutions of [31, 33]

$$1 = \frac{U}{N}\sum_{n\mathbf{k}} \frac{1}{2E_{n\mathbf{k}}}, \tag{14}$$

$$F = 1 - \frac{1}{N}\sum_{n\mathbf{k}} \frac{\xi_{n\mathbf{k}}}{E_{n\mathbf{k}}}, \tag{15}$$

where $N = N_b N_c$ is the total number of lattice sites, with N_b being the number of sublattices in a unit cell. Here, the filling $0 \le F = \frac{1}{N}\sum_{n\mathbf{k}\sigma}\langle c^\dagger_{n\mathbf{k}\sigma} c_{n\mathbf{k}\sigma}\rangle \le 2$ corresponds to the total number of particles per site. Furthermore, the mean-field expression for the filling of condensed particles is given by [31, 33–35]

$$F_c = \frac{1}{N}\sum_{n\mathbf{k}} \frac{\Delta_0^2}{2E_{n\mathbf{k}}^2}. \tag{16}$$

It is known that Eqs. (14), (15) and (16) are sufficient at $T = 0$ to provide a qualitative description of the BCS-BEC crossover for all values of U.

B. Goldstone modes

The dispersions $\omega_{\mathbf{q}}$ of the collective modes are determined by the poles of the fluctuation propagator, as discussed in Appendix A [22, 36]. In the particular case of multiband BCS superconductors with uniform pairing fluctuations [31], and assuming they are below the quasiparticle continuum, the low-energy collective modes are determined by $I^{11}_{\mathbf{q}\omega_{\mathbf{q}}} I^{22}_{\mathbf{q}\omega_{\mathbf{q}}} - \omega_{\mathbf{q}}^2 (I^{12}_{\mathbf{q}\omega_{\mathbf{q}}})^2 = 0$, where

$$I^{11}_{\mathbf{q}\omega} = \frac{2N_b}{U} + \frac{1}{N_c}\sum_{nm\mathbf{k}} \frac{E+E'}{EE'}\frac{EE' + \xi\xi' - \Delta_0^2}{\omega^2 - (E+E')^2} Z, \tag{17}$$

$$I^{22}_{\mathbf{q}\omega} = \frac{2N_b}{U} + \frac{1}{N_c}\sum_{nm\mathbf{k}} \frac{E+E'}{EE'}\frac{EE' + \xi\xi' + \Delta_0^2}{\omega^2 - (E+E')^2} Z, \tag{18}$$

$$I^{12}_{\mathbf{q}\omega} = \frac{1}{N_c}\sum_{nm\mathbf{k}} \left(\frac{\xi}{E} + \frac{\xi'}{E'}\right)\frac{Z}{\omega^2 - (E+E')^2}. \tag{19}$$

Here, we use the shorthand notations $\xi = \xi_{n\mathbf{k}}$, $\xi' = \xi_{m,\mathbf{k}-\mathbf{q}}$, $E = E_{n\mathbf{k}}$, $E' = E_{m,\mathbf{k}-\mathbf{q}}$, and $Z = |\langle n_{\mathbf{k}}|m_{\mathbf{k}-\mathbf{q}}\rangle|^2$ for convenience. In the low-$\mathbf{q}$ limit, $I^{11}_{\mathbf{q}\omega}$ describes the amplitude-amplitude degrees of freedom of the fluctuation propagator, $I^{22}_{\mathbf{q}\omega}$ describes the phase-phase degrees of freedom, and $I^{12}_{\mathbf{q}\omega}$ describes the amplitude-phase coupling. Using Eq. (14), we observe that $I^{22}_{\mathbf{0}\omega} = \frac{1}{N_c}\sum_{n\mathbf{k}}[4E_{n\mathbf{k}}/(\omega^2 - 4E^2_{n\mathbf{k}}) + 1/E_{n\mathbf{k}}]$ vanishes as $\omega \to 0$, indicating that the low-frequency phase mode is always gapless, which allows us to identify it as the in-phase Goldstone mode. Similarly, $I^{11}_{\mathbf{0}\omega}$ vanishes as $\omega \to 2\Delta_0$, again due to Eq. (14), suggesting that the amplitude mode is gapped with energy $2\Delta_0$. This mode is identified as the Higgs mode. While the out-of-phase Leggett modes are not included in this calculation or in the rest of this paper for the sake of simplicity (i.e., they are not analytically tractable in general), this omission is justified in Sec. III D, where it is shown that the Goldstone modes alone exhaust the f-sum rule in the strong-coupling limit.

To determine the collective phonon modes, we expand $I^{11}_{\mathbf{q}\omega} = 2\bar{A} + 2\sum_{ij}\bar{C}_{ij}q_iq_j - 2\bar{D}\omega^2$, $I^{22}_{\mathbf{q}\omega} = 2\sum_{ij}\bar{Q}_{ij}q_iq_j - 2\bar{R}\omega^2$, and $I^{12}_{\mathbf{q}\omega} = -2\bar{B}$ up to second order in $\mathbf{q}$ and ω [31, 36]. The coefficients $\bar{A} = \frac{1}{N_c}\sum_{n\mathbf{k}}\Delta_0^2/(2E^3_{n\mathbf{k}}) = 4\Delta_0^2\bar{R}$, $\bar{B} = \frac{1}{N_c}\sum_{n\mathbf{k}}\xi_{n\mathbf{k}}/(4E^3_{n\mathbf{k}})$ and $\bar{D} = \frac{1}{N_c}\sum_{n\mathbf{k}}\xi^2_{n\mathbf{k}}/(8E^5_{n\mathbf{k}})$ are simply sums of their conventional single-band counterparts. However, the kinetic expansion coefficients $\bar{Q}_{ij} = \bar{Q}^{\mathrm{intra}}_{ij} + \bar{Q}^{\mathrm{inter}}_{ij}$ and $\bar{C}_{ij} = \bar{C}^{\mathrm{intra}}_{ij} + \bar{C}^{\mathrm{inter}}_{ij}$ have both intraband and interband contributions, where

$$\bar{Q}^{\mathrm{intra}}_{ij} = \frac{1}{N_c}\sum_{n\mathbf{k}} \frac{\dot{\xi}^i_{n\mathbf{k}}\dot{\xi}^j_{n\mathbf{k}}}{8E^3_{n\mathbf{k}}}, \tag{20}$$

$$\bar{Q}^{\mathrm{inter}}_{ij} = \frac{1}{N_c}\sum_{n,m\neq n,\mathbf{k}} \frac{(\xi_{n\mathbf{k}} - \xi_{m\mathbf{k}})^2}{8E_{n\mathbf{k}}E_{m\mathbf{k}}(E_{n\mathbf{k}} + E_{m\mathbf{k}})} g^{nm\mathbf{k}}_{ij}, \tag{21}$$

$$\bar{C}^{\mathrm{intra}}_{ij} = \frac{1}{N_c}\sum_{n\mathbf{k}} \left(1 - \frac{5\Delta_0^2\xi^2_{n\mathbf{k}}}{E^4_{n\mathbf{k}}}\right)\frac{\dot{\xi}^i_{n\mathbf{k}}\dot{\xi}^j_{n\mathbf{k}}}{8E^3_{n\mathbf{k}}}, \tag{22}$$

$$\bar{C}^{\mathrm{inter}}_{ij} = -\frac{1}{N_c}\sum_{n\mathbf{k}} \frac{\Delta_0^2}{4E^3_{n\mathbf{k}}} g^{n\mathbf{k}}_{ij} + \frac{1}{N_c}\sum_{n,m\neq n,\mathbf{k}} \frac{(\xi_{n\mathbf{k}} - \xi_{m\mathbf{k}})^2 + 4\Delta_0^2}{8E_{n\mathbf{k}}E_{m\mathbf{k}}(E_{n\mathbf{k}} + E_{m\mathbf{k}})} g^{nm\mathbf{k}}_{ij}. \tag{23}$$

The geometric terms follow from the low-$\mathbf{q}$ expansion of the Bloch factor $Z = |\langle n_{\mathbf{k}}|m_{\mathbf{k}-\mathbf{q}}\rangle|^2$, which can be expressed as

$$Z = \delta_{nm} - \frac{1}{2}\sum_{ij}[g^{n\mathbf{k}}_{ij}\delta_{nm} + g^{nm\mathbf{k}}_{ij}(\delta_{nm} - 1)]q_iq_j, \tag{24}$$

up to second-order in $\mathbf{q}$. Here, $g^{n\mathbf{k}}_{ij} = \sum_{m\neq n} g^{nm\mathbf{k}}_{ij}$ and $g^{nm\mathbf{k}}_{ij} = 2\mathrm{Re}[\langle\dot{n}^i_{\mathbf{k}}|m_{\mathbf{k}}\rangle\langle m_{\mathbf{k}}|\dot{n}^j_{\mathbf{k}}\rangle]$. The separation ensures that the coefficients Q^{intra}_{ij} and C^{intra}_{ij} remain simple sums of their conventional single-band counterparts. Note that $\bar{Q}^{\mathrm{inter}}_{ij}$ and $\bar{C}^{\mathrm{inter}}_{ij}$ do not have any contribution from the band touchings, e.g., the first term of Eq. (23) cancel those touching contributions from the second term whenever $\xi_{n\mathbf{k}} = \xi_{m\mathbf{k}}$ for any $n \neq m$. As a result, the Goldstone modes in the low-$\mathbf{q}$ limit are given by [31, 36]

$$(\omega^G_{\mathbf{q}})^2 = \sum_{ij} \frac{\bar{Q}_{ij}}{\bar{R} + \bar{B}^2/\bar{A}} q_iq_j. \tag{25}$$

These collective modes are related to the superfluid-weight tensor $\mathcal{D}_{ij}$ through $\mathcal{D}_{ij} = \frac{8N_c\Delta_0^2}{V}\bar{Q}_{ij}$ at $T =$

0 [31]. On the other hand, $\bar{C}_{ij}$ is related to the zero-temperature coherence length ξ_0 through $(\xi_0^2)_{ij} = \bar{C}_{ij}/\bar{A}$ [37]. This length scale can, in turn, be connected to the Ginzburg–Landau coherence length in the dilute limit [38, 39].

C. Response functions and f-sum rule

In this section, following Ref. [22], we derive the density and spin response functions for multiband BCS superconductors using the imaginary-time functional path-integral formalism. This approach allows us to calculate the density-density and spin-spin correlation functions by introducing the corresponding source terms. Consequently, after a lengthy but straightforward calculation, the density and spin response functions can be expressed as

$$\mathcal{X}(\mathbf{q},\omega) = \mathcal{X}_s(\mathbf{q},\omega) + 2\Delta_0^2 B_{\mathbf{q}\omega} + \mathcal{X}_c(\mathbf{q},\omega), \tag{26}$$

$$\mathcal{X}_s(\mathbf{q},\omega) = \frac{1}{N_c}\sum_{nm\mathbf{k}} \frac{E+E'}{EE'}\frac{EE'-\xi\xi'-\Delta_0^2}{\omega^2-(E+E')^2}Z, \tag{27}$$

$$\mathcal{X}_c(\mathbf{q},\omega) = \frac{\Delta_0^2 C_{\mathbf{q}\omega}}{\omega^2 (I^{12}_{\mathbf{q}\omega})^2 - I^{11}_{\mathbf{q}\omega} I^{22}_{\mathbf{q}\omega}}, \tag{28}$$

where $C_{\mathbf{q}\omega} = A^2_{\mathbf{q}\omega} I^{22}_{\mathbf{q}\omega} + \omega^2 B^2_{\mathbf{q}\omega} I^{11}_{\mathbf{q}\omega} - 2\omega^2 A_{\mathbf{q}\omega} B_{\mathbf{q}\omega} I^{12}_{\mathbf{q}\omega}$, and $A_{\mathbf{q}\omega} = \frac{1}{N_c}\sum_{nm\mathbf{k}} \frac{E+E'}{EE'}\frac{\xi+\xi'}{\omega^2-(E+E')^2}Z$ and $B_{\mathbf{q}\omega} = \frac{1}{N_c}\sum_{nm\mathbf{k}} \frac{E+E'}{EE'}\frac{Z}{\omega^2-(E+E')^2}$. Similar to the well-known continuum case [21–23], while the density response couples to the collective modes, the spin response does not. In Sec. III B, we show that the collective-mode contribution $\mathcal{X}_c(\mathbf{q},\omega)$ plays a crucial role in the proper description of the BEC regime in the BCS-BEC crossover [40]. Thus, the dynamic SSF and its f-sum rule are simply given by

$$S_s(\mathbf{q},\omega) = \frac{1}{N_c}\sum_{nm\mathbf{k}} \frac{EE'-\xi\xi'-\Delta_0^2}{2EE'} Z\delta(\omega-E-E'), \tag{29}$$

$$\int_0^\infty d\omega\omega S_s(\mathbf{q},\omega) = \frac{1}{N_c}\sum_{nm\mathbf{k}} \frac{E+E'}{2EE'}(EE'-\xi\xi'-\Delta_0^2)Z. \tag{30}$$

Since the SSF is immune to the collective modes, these expressions are valid for any U or $\mathbf{q}$ within the linear-response theory. For instance, it is reassuring to verify that the latter is in perfect agreement with Eqs. (4) and (13) in the low-$\mathbf{q}$ limit, i.e., after using integration by parts $\sum_{\mathbf{k}} \xi_{n\mathbf{k}}\ddot{\xi}^{ij}_{n\mathbf{k}}/E_{n\mathbf{k}} = -\Delta_0^2\sum_{\mathbf{k}} \dot{\xi}^{i}_{n\mathbf{k}}\dot{\xi}^{j}_{n\mathbf{k}}/E^3_{n\mathbf{k}}$ along with the symmetries $g^{nm\mathbf{k}}_{ij} = g^{mn\mathbf{k}}_{ji}$, $g^{n\mathbf{k}}_{ij} = g^{n\mathbf{k}}_{ji}$ and $\sum_{n,m\neq n,\mathbf{k}}(\varepsilon_{n\mathbf{k}}-\varepsilon_{m\mathbf{k}})g^{nm\mathbf{k}}_{ij} = 0$. The static SSF $S_s(\mathbf{q})$ is determined by $\int_0^\infty d\omega S_s(\mathbf{q},\omega) = \frac{1}{N_c}\sum_{nm\mathbf{k}}(EE' - \xi\xi' - \Delta_0^2)Z/(2EE')$ [41]. Note also that $4\mathcal{X}_{\uparrow\downarrow}(\mathbf{q},\omega) = 2\Delta_0^2 B_{\mathbf{q}\omega} + \mathcal{X}_c(\mathbf{q},\omega)$ corresponds to the spin-resolved response function [42].

D. Goldstone contribution

Due to its coupling to the collective phonon modes, the dynamic DSF is quite complicated for high frequencies. However, in the range of frequencies $0 \leq \omega < \Theta$, where $\Theta = \min(E_{n\mathbf{k}}+E_{m,\mathbf{k}-\mathbf{q}})$ is determined by the onset of the quasiparticle continuum, the imaginary parts of $\mathcal{X}_s(\mathbf{q},\omega)$, $I^{11}_{\mathbf{q}\omega}$, $I^{22}_{\mathbf{q}\omega}$, $I^{12}_{\mathbf{q}\omega}$, $A_{\mathbf{q}\omega}$ and $B_{\mathbf{q}\omega}$ vanish when $\omega \to \omega + i0^+$. As a result, the density response function $\mathcal{X}(\mathbf{q},\omega) \to \mathcal{X}_c(\mathbf{q},\omega)$ is determined solely by the collective phase-mode contribution in this frequency interval [43, 44], where we reexpress it as $\mathcal{X}_c(\mathbf{q},\omega) = \frac{\Delta_0^2 C_{\mathbf{q}\omega}}{(I^{12}_{\mathbf{q}\omega})^2}\frac{1}{\omega^2-\Omega^2_{\mathbf{q}\omega}}$. Here, $\Omega_{\mathbf{q}\omega} = \sqrt{I^{11}_{\mathbf{q}\omega} I^{22}_{\mathbf{q}\omega}}/I^{12}_{\mathbf{q}\omega}$, and the collective modes are determined by the condition $\omega_{\mathbf{q}} = \Omega_{\mathbf{q}\omega_{\mathbf{q}}}$. Thus, $S(\mathbf{q},\omega) \to S_c(\mathbf{q},\omega)$ in this frequency interval, where the pole contribution

$$S_c(\mathbf{q},\omega) = \frac{\Delta_0^2 C_{\mathbf{q}\omega^G_{\mathbf{q}}}}{2\omega^G_{\mathbf{q}}(I^{12}_{\mathbf{q}\omega^G_{\mathbf{q}}})^2}\delta(\omega-\omega^G_{\mathbf{q}}) \tag{31}$$

corresponds to the Goldstone modes in the low-$\mathbf{q}$ limit. Using the small $\mathbf{q}$ and ω expansions that are given in Sec. III B, along with $A_{\mathbf{0}0} = -4\bar{B}$ and $B_{\mathbf{0}0} = -4\bar{R}$, we find $C_{\mathbf{q}\omega^G_{\mathbf{q}}} = 32(\bar{A}\bar{R}+\bar{B}^2)\sum_{ij}\bar{Q}_{ij}q_iq_j$, which leads to $S_c(\mathbf{q},\omega) = \frac{V}{2\omega^G_{\mathbf{q}}N_c}(1+\bar{A}\bar{R}/\bar{B}^2)\sum_{ij}\mathcal{D}_{ij}q_iq_j\delta(\omega-\omega^G_{\mathbf{q}})$. In particular, in the strong-coupling limit, one can show that $\bar{A}\bar{R} \ll \bar{B}^2$ and the superfluid-weight tensor can be written as $\mathcal{D}_{ij} = 4\rho_{Cp}(M^{-1}_{Cp})_{ij}$, where $\rho_{Cp} = NF_{Cp}/V$ is the density and $(M^{-1}_{Cp})_{ij}$ is the inverse effective-mass tensor of condensed Cooper pairs [45]. Here, $F_{Cp} = F_c/2$ is the filling of condensed Cooper pairs per lattice site. We have recently shown that $\mathbf{M}_{Cp}$ depends weakly on F, and it is essentially given by the effective-mass tensor $(M^{-1}_{2b})_{ij} = \frac{2}{UN}\sum_{\mathbf{k}}\mathrm{Tr}(\dot{\mathbf{h}}^i_{\mathbf{k}}\dot{\mathbf{h}}^j_{\mathbf{k}})$ of lowest-bound two-body bound states [37]. Thus, in the low-$\mathbf{q}$ limit, the dynamic DSF is dominated by the collective phonon excitations

$$S_c(\mathbf{q},\omega) = 4\frac{N_bF_{Cp}}{2\omega^G_{\mathbf{q}}}\sum_{ij}(M^{-1}_{Cp})_{ij}q_iq_j\delta(\omega-\omega^G_{\mathbf{q}}), \tag{32}$$

up to second-order in $\mathbf{q}$, representing the Goldstone mode of the broken symmetry. Here, N_bF_{Cp} is the filling of condensed Cooper pairs per unit cell.

It is pleasing to see that Eq. (32) recovers the well-known textbook result for the dynamic DSF of a weakly-interacting Bose gas in a continuum model, i.e., it coincides with the phonon contribution within the Bogoliubov approximation [20]. However, note that the resultant density-response function and structure factors are equivalent to four times that of the Cooper pairs, e.g., $\mathcal{X}(\mathbf{q},\omega) \to 4\mathcal{X}_{Cp}(\mathbf{q},\omega)$, since the density of Cooper pairs is $\rho_{Cp}(\mathbf{q},t) = \frac{1}{2}\rho(\mathbf{q},t)$ in the strong-coupling limit [43]. Thus, since $\Theta \to U \gg t$ in this limit, it is important to highlight that the Goldstone contribution alone exhausts

the f-sum rule of the Cooper pairs [43, 44], i.e.,

$$2\int_0^{\Theta} d\omega\omega^{\ell} S_c(\mathbf{q},\omega) = 4\frac{N_b F_{Cp}}{(\omega_{\mathbf{q}}^G)^{1-\ell}}\sum_{ij}(M_{Cp}^{-1})_{ij}q_i q_j \quad (33)$$

when $\ell = 1$. Here, $\ell = -1$ corresponds to the compressibility sum rule, which is also exhausted, while $\ell = 0$ gives the static DSF, which increases linearly with $|\mathbf{q}|$ [20]. Note that the f-sum rule of Eq. (33) can also be written as $\frac{V}{N_c}\sum_{ij}\mathcal{D}_{ij}q_i q_j$, which is consistent with the single-band result [46, 47]. These results indicate that the Goldstone modes are the only relevant degrees of freedom in the low-$\mathbf{q}$ limit at low frequencies. It is also reassuring to verify that Eq. (33) is in perfect agreement with Eq. (13) in the strong-coupling limit. This is because, using $\Delta_0 = \frac{U}{2}\sqrt{F(2-F)}$ and $\mu = -\frac{U}{2}(1-F)$ in this limit, one can reduce $\mathcal{D}_{ij} = \frac{2F(2-F)}{UV}\sum_{\mathbf{k}}\mathrm{Tr}(\dot{\mathbf{h}}_{\mathbf{k}}^i\dot{\mathbf{h}}_{\mathbf{k}}^j)$ [31, 33], where Tr is the trace, and $\sum_{n\mathbf{k}}(M_{n\mathbf{k}}^{-1})_{ij}\big(1-\xi_{n\mathbf{k}}/E_{n\mathbf{k}}\big) \to -\frac{2F(2-F)}{U}\sum_{n\mathbf{k}}(M_{n\mathbf{k}}^{-1})_{ij}\varepsilon_{n\mathbf{k}}$ since $\sum_{n\mathbf{k}}(M_{n\mathbf{k}}^{-1})_{ij} = 0$ in general and $\Delta_0^2/\sqrt{\mu^2+\Delta_0^2}^3 \to 2F(2-F/U$. Furthermore, we can use integration by parts to show that $\sum_{n\mathbf{k}}(M_{n\mathbf{k}}^{-1})_{ij}\varepsilon_{n\mathbf{k}} = \sum_{\mathbf{k}}\mathrm{Tr}(\ddot{\mathbf{h}}_{\mathbf{k}}^{ij}\mathbf{h}_{\mathbf{k}}) = -\sum_{\mathbf{k}}\mathrm{Tr}(\dot{\mathbf{h}}_{\mathbf{k}}^i\dot{\mathbf{h}}_{\mathbf{k}}^j)$. In other words, in the strong-coupling limit of a multiband BCS superconductor, the inverse effective-mass tensor of Cooper pairs can be written as

$$(M_{Cp}^{-1})_{ij} = -\frac{2}{UN}\sum_{n\mathbf{k}}(M_{n\mathbf{k}}^{-1})_{ij}\varepsilon_{n\mathbf{k}}, \quad (34)$$

for which $F_{Cp} = F(2-F)/4$ [31]. Thus, the quantum-geometric origin of the pair mass can be traced all the way back to the effective-mass theorem for Bloch bands, as shown in Eq. (11) [48]. See also Appendix C. Lastly, the exhaustion of the f-sum rule by Eq. (33) suggests that the remaining zeroth-order and second-order contributions to $\mathcal{X}(\mathbf{q},\omega)$ from the high-frequency interval $\Theta \le \omega < \infty$ must necessarily vanish in this limit. See Ref. [22, 23] for an alternative interpretation in a continuum model [49].

IV. NUMERICAL ILLUSTRATION

To illustrate some of our main results, we choose a three-dimensional pyrochlore lattice with a four-point basis [50, 51], described by $h_{\mathbf{k}\sigma}^{SS} = 0$, $h_{\mathbf{k}\sigma}^{AB} = -2\bar{t}\cos\big(\frac{k_y+k_z}{4}a\big)$, $h_{\mathbf{k}\sigma}^{AC} = -2\bar{t}\cos\big(\frac{k_x+k_z}{4}a\big)$, $h_{\mathbf{k}\sigma}^{AD} = -2\bar{t}\cos\big(\frac{k_x+k_y}{4}a\big)$, $h_{\mathbf{k}\sigma}^{BC} = -2\bar{t}\cos\big(\frac{k_x-k_y}{4}a\big)$, $h_{\mathbf{k}\sigma}^{BD} = -2\bar{t}\cos\big(\frac{k_x-k_z}{4}a\big)$ and $h_{\mathbf{k}\sigma}^{CD} = -2\bar{t}\cos\big(\frac{k_y-k_z}{4}a\big)$. Here, $\bar{t}$ is the tight-binding hopping parameter between the nearest-neighbor sites, and a is the side-length of the conventional simple-cubic cell [31]. The crystal structure forms a face-centered-cubic Bravais lattice, resulting in a truncated-octahedron-shaped Brillouin zone (BZ) with a side-length $\sqrt{2}\pi/a$, and the associated reciprocal space is such that $\sum_{\mathbf{k}\in\mathrm{BZ}}1 = N_c$. Consequently, the Bloch spectrum consists of two dispersive bands $\varepsilon_{1\mathbf{k}\sigma} = -2\bar{t}(1+\sqrt{1+\alpha_{\mathbf{k}}})$ and $\varepsilon_{2\mathbf{k}\sigma} = -2\bar{t}(1-\sqrt{1+\alpha_{\mathbf{k}}})$, where $\alpha_{\mathbf{k}} = \cos(k_x a/2)\cos(k_y a/2) + \cos(k_y a/2)\cos(k_z a/2) + \cos(k_x a/2)\cos(k_z a/2)$, and two degenerate flat bands $\varepsilon_{3\mathbf{k}\sigma} = \varepsilon_{4\mathbf{k}\sigma} = 2\bar{t}$. Note that the flat bands touch $\varepsilon_{2\mathbf{k}\sigma}$ at $\mathbf{k} = 0$. In this paper, we set $\bar{t} \to -t$ and choose $t > 0$ as the unit of energy, so that the flat bands appear at the bottom of the Bloch spectrum. It turns out that the pyrochlore lattice is one of the simplest three-dimensional toy models that exhibit a flat band while preserving time-reversal symmetry and uniform pairing. For this reason, in our recent studies, we have also used this model to illustrate the quantum-geometric effects on the superfluid weight, collective modes, coherence length, pair size, and pair mass throughout the BCS-BEC crossover [31, 35, 37]. While those studies also focus on the pyrochlore lattice, they address distinct topics from the present work with only minor overlap.

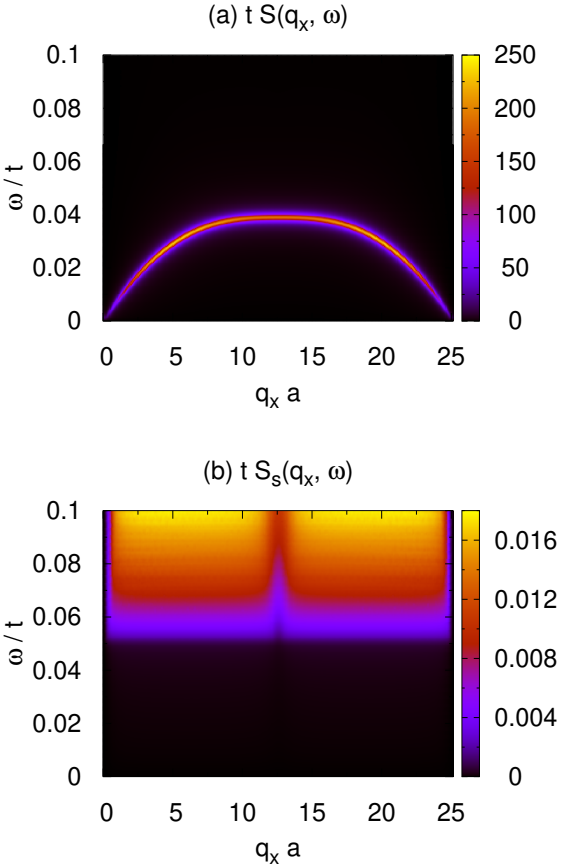

FIG. 1. Half-filled flat bands (i.e., F = 0.5) when $U = 0.1t$, corresponding to $\Delta_0 \approx 0.0253t$ and $\mu \approx -2.00t$. In (a), Goldstone contribution never merges with the quasiparticle continuum, reminiscent of typical BEC behavior. Its energy broadening is controlled by $\eta = 0.001t$.

First of all, when $U = 0$, the region $-2t < \mu < 6t$ lies within the dispersive bands and corresponds to particle fillings $1 < F < 2$, where $\mu = 2t$ is precisely at

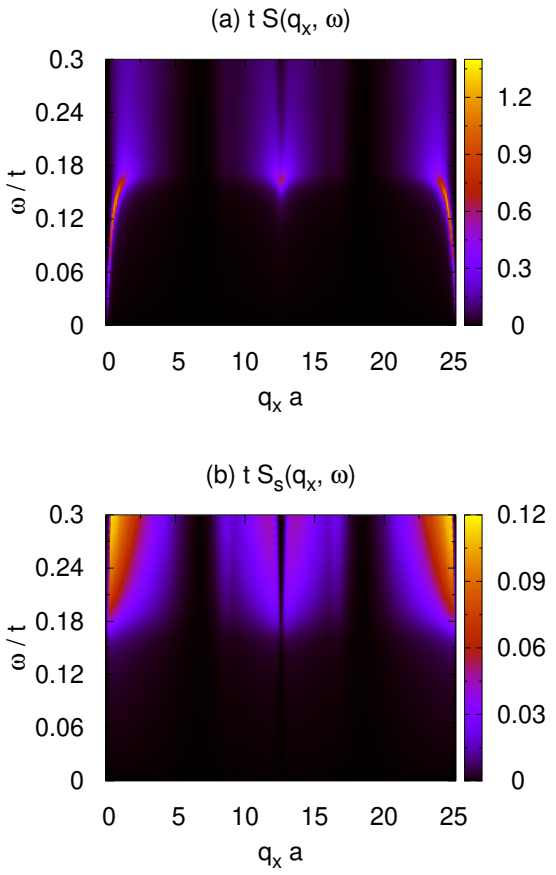

FIG. 2. Partially-filled dispersive bands (i.e., F = 1.25) when $U = 2t$, corresponding to $\Delta_0 \approx 0.0831t$ and $\mu \approx 0.247t$. In (a), Goldstone contribution eventually merges with the quasiparticle continuum at high $\mathbf{q}$, reminiscent of typical BCS behavior. Its energy broadening is controlled by $\eta = 0.01t$.

$F = 1.5$. On the other hand, while $\mu \to -2t$ from above corresponds to a half-filled lattice with $F \to 1$ from above, $\mu = -2t$ coincides with the degenerate flat bands when $0 < F < 1$. Focusing on the flat-band regime, we set $F = 0.5$ in Fig. 1, corresponding to a half-filled flat bands, and present colored maps of the dynamic DSF $-\frac{1}{\pi}\mathrm{Im}\mathcal{X}(\mathbf{q}, \omega + i0^+)$ and the dynamic SSF $-\frac{1}{\pi}\mathrm{Im}\mathcal{X}_s(\mathbf{q}, \omega + i0^+)$ as functions of $\mathbf{q} = (q_x, 0, 0)$ and ω when $U = 0.1t$. Here, the periodicity of the numerical results under $q_x \to q_x + 8\pi/a$ is a reflection of the periodicity of $h^{SS'}_{\mathbf{k}\sigma}$ under $k_x \to k_x + 8\pi/a$. As the dynamic SSF is not coupled to the collective modes, i.e., see Eq. (27), it remains almost featureless at low frequencies until $\omega \sim \Theta$, marking the onset of the quasiparticle continuum in Fig. 1(a), beyond which it exhibits significantly higher intensities. On the other hand, the collective-mode contribution to Eq. (26) is clearly visible as high-intensity peaks throughout momentum space, superimposed on a relatively low background intensity at both low and high frequencies. The fact that the collective mode never merges with the quasiparticle continuum is reminiscent of the BEC-like behavior in the usual BCS-BEC crossover of superfluid Fermi gases [52–54]. This result is also consistent with the Goldstone contribution in Eq. (32), confirming that the Goldstone modes remain undamped even at high $\mathbf{q}$ [55]. Note that, since we represent the Dirac delta function via a Lorentzian distribution $\delta(x) = \frac{1}{\pi}\lim_{\eta\to 0}\frac{\eta}{x^2+\eta^2}$ in our numerics, with $\eta = 0.001t$, the Goldstone modes possess some energy broadening. However, unlike the collective phase modes, the collective amplitude modes (i.e., the Higgs modes) do not leave any visible signature in the dynamic DSF, including the quasiparticle continuum region, where they are expected to decay into pairs of quasiparticle excitations. It is also worth mentioning that, similar to the in-phase Goldstone modes, the out-of-phase Leggett modes are expected to leave strong signatures in the dynamic DSF, at least in the strong-coupling limit where they remain undamped. However, a detailed analysis of these modes is beyond the scope of this paper. In comparison to the flat-band results, we set $F = 1.25$ in Fig. 2, corresponding to partially-filled dispersive bands when $U = 2t$, and show that the collective mode is visible only at low $\mathbf{q}$ in the BCS regime, as it eventually merges with the quasiparticle continuum. This is reminiscent of the BCS-like behavior in the usual BCS-BEC crossover of superfluid Fermi gases [52–54].

V. COULOMB INTERACTION

We now comment on the role of long-range Coulomb interactions among charged particles. In the weak-coupling limit of BCS theory, it is well established that such interactions profoundly alter the collective excitation spectrum. For instance, in three-dimensional systems, instead of supporting a gapless sound mode, the Coulomb interaction pushes the mode to high energies, resulting in a plasma oscillation that lies well above the superconducting gap. Consequently, these collective modes become largely irrelevant except for restoring gauge invariance. As interactions strengthen, however, the superconducting gap increases while the plasma frequency decreases due to the growing effective mass M_{Cp} of tightly bound Cooper pairs. In the extreme strong-coupling (BEC) limit, the system resembles a charged Bose gas, where the plasma frequency approaches zero as M_{Cp} diverges. As discussed in Sec. IV, this behavior also emerges in flat-band superconductors in the $U/t \to 0$ regime. Notably, in contrast to three dimensions, the plasma frequency in two dimensions scales as $\sqrt{|\mathbf{q}|}$ in the long-wavelength limit.

Incorporating Coulomb interactions into the Hubbard model is inherently approximate, as the model treats U as an effective attraction that already accounts for screening and does not explicitly include the bare Coulomb potential. To address this, one typically employs the random-phase approximation (RPA) [56], which yields the following expression for the plasma frequency in the

BEC regime of conventional superconductors:

$$\left(\omega^{P}_{\mathbf{q}\to\mathbf{0}}\right)^2 = V_{Cp}(\mathbf{q})\rho_{Cp}\sum_{ij}\left(M^{-1}_{Cp}\right)_{ij} q_i q_j, \tag{35}$$

where $V_{Cp}(\mathbf{q}) = 2(d-1)\pi e^2_{Cp}/|\mathbf{q}|^{d-1}$ is the Fourier transform of the Coulomb potential for Cooper pairs, $d = \{2, 3\}$ is the dimensionality, and $e_{Cp} = 2e$ is their effective charge. The anisotropy in the plasmon dispersion, governed by the inverse effective-mass tensor $\mathbf{M}^{-1}_{Cp}$, is consistent with recent findings [57]. In isotropic three-dimensional systems, Eq. (35) simplifies to the standard expression $4\pi e^2\mathcal{D}$, also in agreement with the literature [58]. Given our analysis in Sec. IV, we expect Eq. (35) to remain valid for flat-band superconductors, owing to their strongly interacting nature even in the $U/t \to 0$ regime.

VI. CONCLUSION

In summary, we explored the interplay between quantum geometry and superconductivity in multiband BCS systems that exhibit time-reversal symmetry and uniform pairing. Using linear-response theory within the mean-field BCS-BEC crossover framework at $T = 0$, we analyzed the dynamic DSF and dynamic SSF of a multi-orbital Hubbard model. Our results rigorously satisfy the associated f-sum rules across various limits. Notably, in the strong-coupling regime, the behavior converges to that of a weakly-interacting Bose gas of Cooper pairs, with low-energy collective Goldstone modes emerging as Bogoliubov phonons. We further demonstrated that the quantum-geometric origin of these low-energy structure factors, and related observables such as the superfluid-weight tensor and the effective-mass tensor of Cooper pairs, can be traced back to the effective-mass theorem for Bloch bands. As an illustrative example, we investigate the pyrochlore-Hubbard model numerically, highlighting the profound impact of quantum geometry through collective Goldstone modes on the superconducting properties of a complex flat-band lattice. As an outlook, future studies could explore the contribution of collective Leggett modes to the dynamic DSF, as these out-of-phase modes are expected to play some role away from the strong-coupling limit toward the BCS-BEC crossover regime. For instance, in a multiband lattice with N_b sublattices, we anticipate the emergence of $N_b - 1$ distinct Leggett branches, all of which can be investigated numerically by introducing a sublattice-dependent order parameter for the fluctuations [31]. Studying the effects of finite temperature is also crucial. However, even in a single-band lattice or continuum model, a significant theoretical challenge arises due to the presence of Landau singularities in the $(\mathbf{q}, \omega) \to (\mathbf{0}, 0)$ limit, which lead to the damping of even the low-energy collective modes [59].

ACKNOWLEDGMENTS

The author acknowledges funding from US Air Force Office of Scientific Research (AFOSR) Grant No. FA8655-24-1-7391.

Appendix A: Gaussian fluctuations

In the case of multiband BCS superconductors with uniform pairing fluctuations, the effective Gaussian action can be written as [22, 31, 36]

$$\mathcal{S}_{\rm GF} = \frac{1}{2}\sum_q \left(\Lambda^*_q\, \Lambda_{-q}\right)\begin{pmatrix} \mathcal{M}^{11}_q & \mathcal{M}^{12}_q \\ \mathcal{M}^{21}_q & \mathcal{M}^{22}_q \end{pmatrix}\begin{pmatrix} \Lambda_q \\ \Lambda^*_{-q} \end{pmatrix}, \tag{A1}$$

where $q \equiv (\mathbf{q}, iq_\ell)$ is a combined index with $q_\ell = 2\ell\pi T$ the bosonic Matsubara frequency, Λ_q describes fluctuations of the order parameter field around its saddle-point value Δ_0, and the fluctuation matrix $\boldsymbol{\mathcal{M}}_q$ acts as an inverse propagator. Denoting $u^2 = (1+\xi/E)/2$, $u'^2 = (1+\xi'/E')/2$, $v^2 = (1-\xi/E)/2$ and $v'^2 = (1-\xi'/E')/2$, the matrix elements $\mathcal{M}^{12}_q = \mathcal{M}^{21}_q$ and $\mathcal{M}^{11}_q = \mathcal{M}^{22}_{-q}$ can be written as

$$\mathcal{M}^{11}_q = \frac{N_S}{U} + \frac{1}{N_c}\sum_{nm\mathbf{k}}\left(\frac{u^2u'^2}{iq_\ell - E - E'} - \frac{v^2v'^2}{iq_\ell + E + E'}\right)Z, \tag{A2}$$

$$\mathcal{M}^{12}_q = \frac{1}{N_c}\sum_{nm\mathbf{k}}\left(\frac{uvu'v'}{iq_\ell + E + E'} - \frac{uvu'v'}{iq_\ell - E - E'}\right)Z, \tag{A3}$$

at $T = 0$. Next we introduce the transformation $\Lambda_q = \lambda_{1,q} + i\lambda_{2,q}$, and associate $\lambda_{1,q} = \lambda^*_{1,-q}$ and $\lambda_{2,q} = \lambda^*_{2,-q}$ with the amplitude and phase degrees of freedom, respectively. This leads to the following expressions for the effective couplings in the Gaussian action: $I^{11}_q = \mathcal{M}^{11}_q + \mathcal{M}^{22}_q + \mathcal{M}^{12}_q + \mathcal{M}^{21}_q$ for the amplitude-amplitude, $I^{22}_q = \mathcal{M}^{11}_q + \mathcal{M}^{22}_q - \mathcal{M}^{12}_q - \mathcal{M}^{21}_q$ for the phase-phase, and $q_\ell I^{12}_q = i(\mathcal{M}^{11}_q - \mathcal{M}^{22}_q - \mathcal{M}^{12}_q + \mathcal{M}^{21}_q)$ for the amplitude-phase. With these, the effective Gaussian action becomes

$$\mathcal{S}_{\rm GF} = \frac{1}{2}\sum_q \left(\lambda_{1,-q}\, \lambda_{2,-q}\right)\begin{pmatrix} I^{11}_q & q_\ell I^{12}_q \\ -q_\ell I^{12}_q & I^{22}_q \end{pmatrix}\begin{pmatrix} \lambda_{1,q} \\ \lambda_{2,q} \end{pmatrix}. \tag{A4}$$

In Sec. III B, $I^{ij}_{\mathbf{q}\omega}$ denotes I^{ij}_q after analytic continuation $iq_\ell \to \omega$.

Appendix B: Ward identities

The Ward identities for the density response functions given in Ref. [23] can be easily generalized to the case of multiband BCS superconductors. At $T = 0$, their Eq. (42) is analogous to the following expressions

$$\frac{1}{N_c}\sum_{nm\mathbf{k}}\frac{E+E'}{EE'}\frac{(\xi+\xi')Z}{\omega^2-(E+E')^2}-\frac{2}{N_c}\sum_{nm\mathbf{k}}\left(\frac{\xi}{E}+\frac{\xi'}{E'}\right)\frac{Z}{\omega^2-(E+E')^2}=\frac{1}{N_c}\sum_{nm\mathbf{k}}\frac{E-E'}{EE'}\frac{(\xi-\xi')Z}{\omega^2-(E+E')^2}, \tag{B1}$$

$$\frac{1}{N_c}\sum_{nm\mathbf{k}}\frac{E+E'}{EE'}\frac{\omega^2 Z}{\omega^2-(E+E')^2}-2\left[\frac{2N_b}{U}+\frac{1}{N_c}\sum_{nm\mathbf{k}}\frac{E+E'}{EE'}\frac{EE'+\xi\xi'+\Delta_0^2}{\omega^2-(E+E')^2}Z\right]=\frac{1}{N_c}\sum_{nm\mathbf{k}}\frac{E+E'}{EE'}\frac{(\xi-\xi')^2 Z}{\omega^2-(E+E')^2}, \tag{B2}$$

$$\frac{1}{N_c}\sum_{nm\mathbf{k}}\frac{E+E'}{EE'}\frac{EE'-\xi\xi'+\Delta_0^2}{\omega^2-(E+E')^2}Z-\frac{1}{N_c}\sum_{nm\mathbf{k}}\frac{E+E'}{EE'}\frac{2\Delta_0^2 Z}{\omega^2-(E+E')^2}=\frac{1}{N_c}\sum_{nm\mathbf{k}}\left(\frac{\xi}{E}-\frac{\xi'}{E'}\right)\frac{(\xi-\xi')Z}{\omega^2-(E+E')^2}. \tag{B3}$$

These identities can be verified through algebraic manipulations, e.g., the second identity can be shown via the substitution $4N/U=\sum_{nm\mathbf{k}}(Z/E+Z/E')$, which follows from the order-parameter Eq. (14).

Appendix C: Effective-mass tensors

Note that the inverse effective-mass tensor $\mathbf{M}_{n\mathbf{k}}^{-1}$ for the nth Bloch band [27] and the inverse effective-mass tensor $\mathbf{M}_{2b}^{-1}$ for the lowest-lying two-body bound states [60] can be written compactly as

$$(M_{n\mathbf{k}}^{-1})_{ij}=\sum_m (f_{nm\mathbf{k}}^{-1})_{ij}, \tag{C1}$$

$$(M_{2b}^{-1})_{ij}=\frac{\sum_{nm\mathbf{k}}\frac{(f_{nm\mathbf{k}}^{-1})_{ij}-\ddot{\varepsilon}_{n\mathbf{k}}^{ij}\delta_{nm}/2}{(2\varepsilon_{n\mathbf{k}}-E_b)(\varepsilon_{n\mathbf{k}}+\varepsilon_{m\mathbf{k}}-E_b)}}{\sum_{n\mathbf{k}}\frac{1}{(2\varepsilon_{n\mathbf{k}}-E_b)^2}}, \tag{C2}$$

where $E_b<0$, with $|E_b|$ denoting the binding energy of the pair, and

$$(f_{nm\mathbf{k}}^{-1})_{ij}=\ddot{\varepsilon}_{n\mathbf{k}}^{ij}\delta_{nm}-(\varepsilon_{n\mathbf{k}}-\varepsilon_{m\mathbf{k}})g_{ij}^{nm\mathbf{k}} \tag{C3}$$

can be interpreted as the band-resolved inverse effective-mass tensor for the nth Bloch band. Then, it is again reassuring to verify that Eq. (C2) is in perfect agreement with Eq. (34) in the $U\gg t$ limit, where $|E_b|\to U\gg\max\{2\varepsilon_{n\mathbf{k}}\}$. To show this, we make use of the following identities: $\sum_{n\mathbf{k}}\ddot{\varepsilon}_{n\mathbf{k}}^{ij}=0$, $g_{ij}^{nm\mathbf{k}}=g_{ji}^{mn\mathbf{k}}$, $g_{ij}^{n\mathbf{k}}=g_{ji}^{n\mathbf{k}}$ and $\sum_{n,m\neq n}\varepsilon_{m\mathbf{k}}g_{ij}^{nm\mathbf{k}}=\sum_n\varepsilon_{n\mathbf{k}}g_{ij}^{n\mathbf{k}}$. This correspondence further illustrates the quantum-geometric origin of the pair mass. Notably, a similar geometric contribution has also been reported for the optical mass [16].

[1] X. Tan, D.-W. Zhang, Z. Yang, J. Chu, Y.-Q. Zhu, D. Li, X. Yang, S. Song, Z. Han, Z. Li, Y. Dong, H.-F. Yu, H. Yan, S.-L. Zhu, and Y. Yu, Experimental measurement of the quantum metric tensor and related topological phase transition with a superconducting qubit, Phys. Rev. Lett. **122**, 210401 (2019).

[2] M. Yu, P. Yang, M. Gong, Q. Cao, Q. Lu, H. Liu, S. Zhang, M. B. Plenio, F. Jelezko, T. Ozawa, *et al.*, Experimental measurement of the quantum geometric tensor using coupled qubits in diamond, National science review **7**, 254 (2020).

[3] A. Gianfrate, O. Bleu, L. Dominici, V. Ardizzone, M. De Giorgi, D. Ballarini, G. Lerario, K. West, L. Pfeiffer, D. Solnyshkov, *et al.*, Measurement of the quantum geometric tensor and of the anomalous Hall drift, Nature **578**, 381 (2020).

[4] H. Tian, X. Gao, Y. Zhang, S. Che, T. Xu, P. Cheung, K. Watanabe, T. Taniguchi, M. Randeria, F. Zhang, *et al.*, Evidence for Dirac flat band superconductivity enabled by quantum geometry, Nature **614**, 440 (2023).

[5] C.-R. Yi, J. Yu, H. Yuan, R.-H. Jiao, Y.-M. Yang, X. Jiang, J.-Y. Zhang, S. Chen, and J.-W. Pan, Extracting the quantum geometric tensor of an optical raman lattice by bloch-state tomography, Phys. Rev. Res. **5**, L032016 (2023).

[6] A. Gao, Y.-F. Liu, J.-X. Qiu, B. Ghosh, T. V. Trevisan, Y. Onishi, C. Hu, T. Qian, H.-J. Tien, S.-W. Chen, *et al.*, Quantum metric nonlinear Hall effect in a topological antiferromagnetic heterostructure, Science **381**, 181 (2023).

[7] S. Kim, Y. Chung, Y. Qian, S. Park, C. Jozwiak, E. Rotenberg, A. Bostwick, K. S. Kim, and B.-J. Yang, Direct measurement of the quantum metric tensor in solids, Science **388**, 1050 (2025).

[8] G. Sala, M. T. Mercaldo, K. Domi, S. Gariglio, M. Cuoco, C. Ortix, and A. D. Caviglia, The quantum metric of electrons with spin-momentum locking, arXiv preprint arXiv:2407.06659 (2024).

[9] M. Kang, S. Kim, Y. Qian, P. M. Neves, L. Ye, J. Jung, D. Puntel, F. Mazzola, S. Fang, C. Jozwiak, *et al.*, Measurements of the quantum geometric tensor in solids, Nature Physics , 1 (2024).

[10] M. Tanaka, J. Î. Wang, T. H. Dinh, D. Rodan-Legrain, S. Zaman, M. Hays, B. Kannan, A. Almanakly, D. K. Kim, B. M. Niedzielski, *et al.*, Superfluid stiffness and flat-band superconductivity in magic-angle graphene probed by cQED, arXiv preprint arXiv:2406.13740 (2024).

[11] J. P. Provost and G. Vallee, Riemannian structure on manifolds of quantum states, Commun. Math. Phys. **76**, 289 (1980).

[12] M. V. Berry, Quantal phase factors accompanying adiabatic changes, Proceedings of the Royal Society of London. A. Mathematical and Physical Sciences **392**, 45 (1984).

[13] R. Resta, The insulating state of matter: a geometrical theory, The European Physical Journal B **79**, 121 (2011).

[14] P. Törmä, S. Peotta, and B. A. Bernevig, Superconductivity, superfluidity and quantum geometry in twisted multilayer systems, Nature Reviews Physics **4**, 528 (2022).

[15] P. Törmä, Essay: Where can quantum geometry lead us?, Phys. Rev. Lett. **131**, 240001 (2023).

[16] J. Yu, B. A. Bernevig, R. Queiroz, E. Rossi, P. Törmä, and B.-J. Yang, Quantum geometry in quantum materials, arXiv preprint arXiv:2501.00098 (2024).

[17] Y. Jiang, T. Holder, and B. Yan, Revealing quantum geometry in nonlinear quantum materials, Reports on Progress in Physics (2025).

[18] Y. Onishi and L. Fu, Topological bound on the structure factor, Phys. Rev. Lett. **133**, 206602 (2024).

[19] Y. Onishi, A. Avdoshkin, and L. Fu, Geometric bound on structure factor, arXiv preprint arXiv:2412.02656 (2024).

[20] P. Nozieres and D. Pines, *Theory Of Quantum Liquids*, Advanced Books Classics (Avalon Publishing, 1999).

[21] R. Combescot, S. Giorgini, and S. Stringari, Molecular signatures in the structure factor of an interacting Fermi gas, Europhysics Letters **75**, 695 (2006).

[22] L. He, Dynamic density and spin responses of a superfluid Fermi gas in the BCS–BEC crossover: Path integral formulation and pair fluctuation theory, Annals of Physics **373**, 470 (2016).

[23] H. Guo, C.-C. Chien, and Y. He, Theories of linear response in BCS superfluids and how they meet fundamental constraints, Journal of Low Temperature Physics **172**, 5 (2013).

[24] T. Kitamura, A. Daido, and Y. Yanase, Spin-triplet superconductivity from quantum-geometry-induced ferromagnetic fluctuation, Phys. Rev. Lett. **132**, 036001 (2024).

[25] For instance, by making use of the commutator relation $[\rho_{S\mathbf{q}\sigma},\mathcal{H}_0] = \frac{1}{\sqrt{N_c}}\sum_{nm\mathbf{k}}(\varepsilon_{m\mathbf{k}\sigma} - \varepsilon_{n,\mathbf{k}-\mathbf{q},\sigma})n^*_{S,\mathbf{k}-\mathbf{q},\sigma}m_{S\mathbf{k}\sigma}c^\dagger_{n,\mathbf{k}-\mathbf{q},\sigma}c_{m\mathbf{k}\sigma}$, where the non-interacting Hamiltonian $\mathcal{H}_0$ is given in Eq. (7), one can show that $[\rho_{S'\mathbf{q}'\sigma'},[\rho_{S\mathbf{q}\sigma},\mathcal{H}_0] = \frac{\delta_{\sigma\sigma'}}{N_c}\sum_{nml\mathbf{k}}(\varepsilon_{m\mathbf{k}\sigma} - \varepsilon_{n,\mathbf{k}-\mathbf{q},\sigma})n^*_{S,\mathbf{k}-\mathbf{q},\sigma}m_{S\mathbf{k}\sigma}(l^*_{S',\mathbf{k}-\mathbf{q}-\mathbf{q}',\sigma}n_{S',\mathbf{k}-\mathbf{q},\sigma}c^\dagger_{l,\mathbf{k}-\mathbf{q}-\mathbf{q}',\sigma}c_{m\mathbf{k}\sigma} - m^*_{S'\mathbf{k}\sigma}l_{S',\mathbf{k}+\mathbf{q}',\sigma}c^\dagger_{n,\mathbf{k}-\mathbf{q},\sigma}c_{l,\mathbf{k}+\mathbf{q}',\sigma})$.

[26] In general, the low-$\mathbf{q}$ limit can be written as $[\rho^\dagger_{\mathbf{q}},[\rho_{\mathbf{q}},\mathcal{H}]] = -\frac{1}{N_c}\sum_{ijnm\mathbf{k}\sigma}(M^{-1}_{nm\mathbf{k}\sigma})_{ij}q_iq_jc^\dagger_{n\mathbf{k}\sigma}c_{m\mathbf{k}\sigma}$, up to second-order in $\mathbf{q}$, where the coefficients for the inverse effective-mass tensor are given by $(M^{-1}_{nm\mathbf{k}\sigma})_{ij} = \ddot{\varepsilon}^{ij}_{n\mathbf{k}\sigma}\delta_{nm} + 2(\dot{\varepsilon}^i_{n\mathbf{k}\sigma} - \dot{\varepsilon}^i_{m\mathbf{k}\sigma})\langle\dot{n}^j_{\mathbf{k}\sigma}|m_{\mathbf{k}\sigma}\rangle + (\varepsilon_{n\mathbf{k}\sigma} - \varepsilon_{m\mathbf{k}\sigma})(\langle\ddot{n}^{ij}_{\mathbf{k}\sigma}|m_{\mathbf{k}\sigma}\rangle + \langle\dot{n}^i_{\mathbf{k}\sigma}|\dot{m}^j_{\mathbf{k}\sigma}\rangle) + \sum_l(2\varepsilon_{l\mathbf{k}\sigma} - \varepsilon_{n\mathbf{k}\sigma} - \varepsilon_{m\mathbf{k}\sigma})\langle\dot{l}^i_{\mathbf{k}\sigma}|m_{\mathbf{k}\sigma}\rangle\langle n_{\mathbf{k}\sigma}|\dot{l}^j_{\mathbf{k}\sigma}\rangle$.

[27] M. Iskin, Geometric mass acquisition via a quantum metric: An effective-band-mass theorem for the helicity bands, Phys. Rev. A **99**, 053603 (2019).

[28] Y. Onishi and L. Fu, Fundamental bound on topological gap, Phys. Rev. X **14**, 011052 (2024).

[29] N. Verma and R. Queiroz, Instantaneous response and quantum geometry of insulators, arXiv preprint arXiv:2403.07052 (2024).

[30] L. Liang, T. I. Vanhala, S. Peotta, T. Siro, A. Harju, and P. Törmä, Band geometry, Berry curvature, and superfluid weight, Phys. Rev. B **95**, 024515 (2017).

[31] M. Iskin, Cooper pairing, flat-band superconductivity, and quantum geometry in the pyrochlore-Hubbard model, Phys. Rev. B **109**, 174508 (2024).

[32] P. Nozieres and S. Schmitt-Rink, Bose condensation in an attractive fermion gas: From weak to strong coupling superconductivity, Journal of Low Temperature Physics **59**, 195 (1985).

[33] M. Iskin, Berezinskii-Kosterlitz-Thouless transition in the time-reversal-symmetric Hofstadter-Hubbard model, Phys. Rev. A **97**, 013618 (2018).

[34] A. Leggett, *Quantum Liquids: Bose condensation and Cooper pairing in condensed-matter systems* (Oxford University Press, United Kingdom, 2008) publisher Copyright: © Oxford University Press, 2014.

[35] M. Iskin, Pair size and quantum geometry in a multiband Hubbard model, Phys. Rev. B **111**, 014502 (2025).

[36] J. R. Engelbrecht, M. Randeria, and C. A. R. Sáde Melo, BCS to Bose crossover: Broken-symmetry state, Phys. Rev. B **55**, 15153 (1997).

[37] M. Iskin, Coherence length and quantum geometry in a dilute flat-band superconductor, Phys. Rev. B **110**, 144505 (2024).

[38] S. A. Chen and K. T. Law, Ginzburg-Landau theory of flat-band superconductors with quantum metric, Phys. Rev. Lett. **132**, 026002 (2024).

[39] M. Iskin, Extracting quantum-geometric effects from Ginzburg-Landau theory in a multiband Hubbard model, Phys. Rev. B **107**, 224505 (2023).

[40] We also note that, if we ignore the collective-mode contribution $\mathcal{X}_c(\mathbf{q},\omega)$ and set it to zero, the compressibility sum rule $2\int_0^\infty\frac{d\omega}{\omega}S(\mathbf{q},\omega) = \frac{1}{N_c}\sum_{n\mathbf{k}}\Delta_0^2/E^3_{n\mathbf{k}} = N_b\partial F/\partial\mu$ is satisfied at the mean-field level, where N_bF is the particle filling per unit cell.

[41] The low-$\mathbf{q}$ expansion of the static SSF $S_s(\mathbf{q})$ can be determined as $\int_0^\infty d\omega S_s(\mathbf{q},\omega) = \sum_{ij}\frac{q_iq_j}{N_c}[\Delta_0^2\sum_{n\mathbf{k}}\dot{\xi}^i_{n\mathbf{k}}\dot{\xi}^j_{n\mathbf{k}}/(4E^4_{n\mathbf{k}}) + \sum_{n,m\neq n,\mathbf{k}}(E_{n\mathbf{k}}E_{m\mathbf{k}} - \xi_{n\mathbf{k}}\xi_{m\mathbf{k}} - \Delta_0^2)g^{nm\mathbf{k}}_{ij}/(4E_{n\mathbf{k}}E_{m\mathbf{k}})]$.

[42] Note that the $B_{\mathbf{q}\omega}$-term has the following contributions to the f-sum rule $-\frac{1}{\pi}\int_0^\infty d\omega\omega\mathrm{Im}B_{\mathbf{q},\omega+i0^+} = 2N_b/U$ and static DSF $-\frac{1}{\pi}\int_0^\infty d\omega\mathrm{Im}B_{\mathbf{q},\omega+i0^+} = \frac{1}{2N_c}\sum_{n\mathbf{k}}1/E^2_{n\mathbf{k}} - \sum_{ij}\frac{q_iq_j}{4N_c}[\sum_{n\mathbf{k}}\dot{\xi}^i_{n\mathbf{k}}\dot{\xi}^j_{n\mathbf{k}}\xi^2_{n\mathbf{k}}/E^6_{n\mathbf{k}} - \sum_{n,m\neq n,\mathbf{k}}g^{nm\mathbf{k}}_{ij}/(E_{n\mathbf{k}}E_{m\mathbf{k}})]$ up to second-order in $\mathbf{q}$.

[43] H. P. Büchler, P. Zoller, and W. Zwerger, Spectroscopy of superfluid pairing in atomic Fermi gases, Phys. Rev. Lett. **93**, 080401 (2004).

[44] M. T. Mitchison, T. H. Johnson, and D. Jaksch, Probing the dynamic structure factor of a neutral Fermi superfluid along the BCS-BEC crossover using atomic impurity qubits, Phys. Rev. A **94**, 063618 (2016).

[45] Recall that the superfluid-weight tensor is $\mathcal{D}_{ij} = \frac{8N_c\Delta_0^2}{V}\bar{Q}_{ij}$, where the expansion coefficient $\bar{Q}_{ij} = \bar{Q}_{ij}^{\text{intra}} + \bar{Q}_{ij}^{\text{inter}}$ can alternatively be expressed as $\bar{Q}_{ij}^{\text{intra}} = \frac{1}{8\Delta_0^2 N_c}\sum_{n\mathbf{k}}(1 - \xi_{n\mathbf{k}}/E_{n\mathbf{k}})\ddot{\xi}_{n\mathbf{k}}^{ij}$, since $\sum_{\mathbf{k}}\ddot{\xi}_{n\mathbf{k}}^{ij} = 0$, and $\bar{Q}_{ij}^{\text{inter}} = \frac{1}{4N_c}\sum_{n\mathbf{k}} g_{ij}^{n\mathbf{k}}/E_{n\mathbf{k}} - \frac{1}{2N_c}\sum_{n,m\neq n,\mathbf{k}}\xi_{m\mathbf{k}}g_{ij}^{nm\mathbf{k}}/[E_{m\mathbf{k}}(\xi_{n\mathbf{k}} + \xi_{m\mathbf{k}})]$. In the strong-coupling limit, they can be approximated as $\bar{Q}_{ij}^{\text{intra}} = \frac{1}{16N_c}\sum_{n\mathbf{k}}\ddot{\xi}_{n\mathbf{k}}^{ij}/\xi_{n\mathbf{k}}^2$ and $\bar{Q}_{ij}^{\text{inter}} = \frac{1}{4N_c}\sum_{n\mathbf{k}} g_{ij}^{n\mathbf{k}}/|\xi_{n\mathbf{k}}| - \frac{1}{2N_c}\sum_{n,m\neq n,\mathbf{k}} g_{ij}^{nm\mathbf{k}}/(|\xi_{n\mathbf{k}}| + |\xi_{m\mathbf{k}}|)$, showing direct relation to the effective-mass tensor of Cooper pairs [31].

[46] H. Monien and K. S. Bedell, Collective excitations and sum rules for the Hubbard model in the spin-density-wave regime, Phys. Rev. B **45**, 3164 (1992).

[47] P. J. H. Denteneer, G. An, and J. M. J. van Leeuwen, Helicity modulus in the two-dimensional Hubbard model, Phys. Rev. B **47**, 6256 (1993).

[48] By reexpressing the superfluid-weight tensor as $\mathcal{D}_{ij} = -\frac{2F(2-F)}{UV}\sum_{n\mathbf{k}}(M_{n\mathbf{k}}^{-1})_{ij}\varepsilon_{n\mathbf{k}}$, we conclude that its quantum-geometric origin is also directly linked to Eq. (11), i.e., to the effective-mass theorem for Bloch bands [27], in the strong-coupling limit.

[49] In Ref. [23], we observed a crucial flaw in the argument used in the proof of the f-sum rule. Specifically, in Eq. (53), they erroneously claim that the integral vanishes because the integrand is odd in ω. However, by similar reasoning, one could argue that Eq. (49) is even in ω, which would imply that the integral of $\text{Im}(\omega K^{00})$ should also vanish entirely. We thank C.-C. Chien for their email correspondence on this particular issue.

[50] J. P. Wakefield, M. Kang, P. M. Neves, D. Oh, S. Fang, R. McTigue, S. Frank Zhao, T. N. Lamichhane, A. Chen, S. Lee, *et al.*, Three-dimensional flat bands in pyrochlore metal CaNi2, Nature **623**, 301 (2023).

[51] J. Huang, C. Setty, L. Deng, J.-Y. You, H. Liu, S. Shao, J. S. Oh, Y. Guo, Y. Zhang, Z. Yue, *et al.*, Observation of flat bands and Dirac cones in a pyrochlore lattice superconductor, npj Quantum Materials **9**, 71 (2024).

[52] P. Zou, F. Dalfovo, R. Sharma, X.-J. Liu, and H. Hu, Dynamic structure factor of a strongly correlated Fermi superfluid within a density functional theory approach, New Journal of Physics **18**, 113044 (2016).

[53] S. Hoinka, P. Dyke, M. G. Lingham, J. J. Kinnunen, G. M. Bruun, and C. J. Vale, Goldstone mode and pair-breaking excitations in atomic Fermi superfluids, Nature Physics **13**, 943 (2017).

[54] H. Biss, L. Sobirey, N. Luick, M. Bohlen, J. J. Kinnunen, G. M. Bruun, T. Lompe, and H. Moritz, Excitation spectrum and superfluid gap of an ultracold Fermi gas, Phys. Rev. Lett. **128**, 100401 (2022).

[55] Similar to the strong-coupling limit discussed in Sec. III D, one can also show that in the dilute limit of the pyrochlore lattice, i.e., when $F \to 0$, the inequality $\bar{A}\bar{R} \ll \bar{B}^2$ holds for any $U \neq 0$ [31]. Furthermore, the superfluid-weight tensor again takes the form $\mathcal{D}_{ij} = 4\rho_{Cp}(M_{Cp}^{-1})_{ij}$, where both ρ_{Cp} and $(M_{Cp}^{-1})_{ij}$ depend on U [31]. As a result, Eq. (32) also holds for any $U \neq 0$ in the dilute flat-band regime.

[56] L. Belkhir and M. Randeria, Crossover from Cooper pairs to composite bosons: A generalized RPA analysis of collective excitations, Phys. Rev. B **49**, 6829 (1994).

[57] S. Ahn and S. Das Sarma, Theory of anisotropic plasmons, Phys. Rev. B **103**, L041303 (2021).

[58] F. Gabriele, C. Castellani, and L. Benfatto, Generalized plasma waves in layered superconductors: A unified approach, Phys. Rev. Res. **4**, 023112 (2022).

[59] H. Kurkjian, S. N. Klimin, J. Tempere, and Y. Castin, Pair-breaking collective branch in BCS superconductors and superfluid Fermi gases, Phys. Rev. Lett. **122**, 093403 (2019).

[60] M. Iskin, Effective-mass tensor of the two-body bound states and the quantum-metric tensor of the underlying Bloch states in multiband lattices, Phys. Rev. A **105**, 023312 (2022).